MULTI-SENSOR DATA FUSION FOR INTEGRATED NAVIGATION SYSTEMS OF SMALL AUTONOMOUS UNMANNED AIRCRAFT

S. Winkler, P. Vörsmann

Institute of Aerospace Systems
Technical University of Braunschweig
Hermann-Blenk-Straße 23, D-38108 Braunschweig, Germany

ABSTRACT

This paper presents a solution for reliable and high-frequent state determination of small unmanned aircraft. It is a tightly-coupled GPS/INS navigation system in which a MEMS-INS is aided by a commercial low-cost stand-alone single-antenna L1 GPS-receiver. The aiding with carrier phases is done by non conventional algorithms. Instead of solving for the integer ambiguities, time-differenced carrier phases are used.

For GPS/INS integration a Kalman filter is developed and simplified for the use of low-cost sensors. An observability analysis is done for the simplified system. Instead of processing delta-ranges, an analysis is carried out to replace them by time-differenced carrier phases. The corresponding measurement model for the navigation filter is derived. Finally, the new navigation algorithms are validated in drive tests and flight tests and compared to the conventional ones.

1 INTRODUCTION

Following the realization of automatic flights of small unmanned aircraft [e.g. 1; 2], current efforts are focused on the improvement of flight performance and quality in autonomous mode as well as their usage for sophisticated applications. For this a reliable and high-frequent attitude information is most often obligatory. Instead of directly measuring, observing the attitude based on inertial sensors and satellite navigation receivers within integrated navigation systems has turned out to be an appropriate solution. In this work a theoretical and experimental research is conducted for the integration of low-cost satellite and inertial navigation systems for small unmanned aircraft.

The field of applications of unmanned aerial vehicles (UAV) is huge. The most important applications of the presented work are:

1. high-dynamic automatic flight of small UAVs,
2. wind vector measuring by small UAVs.

For both applications a reliable and high-frequent attitude information is of significant importance. In the first application, it is essential in order to completely use the aircraft's aerodynamic abilities. Hence, in automatic mode it can still fly very agile (e.g. with minimum curve radii). This is not possible without attitude information. In the second application the attitude is necessary in order to transform the air flow velocity vector, measured aircraft-fixed, into the geodetic coordinate frame where wind computation is usually done.

The considered UAVs have a wing span of up to about 3.5 m and a maximum take-off weight of up to about 6 kg. Due to limimations in mass, volume and energy capacities on-board the aircraft, only miniaturized sensors are applicable. Furthermore, in order to minimize hardware costs, only off-the-shelf sensors available on the free marked are to be used. Concerning the navigation algorithms, their real-time capability on a miniaturized on-board computer must be ensured. With this a continuous telemetrie link between aircraft and ground station in order to realize the automatic flight can be avoided which increases the system reliability.

A low-cost integrated navigation system for small UAVs is developed and validated in experiments. It is based on a tightly-coupled low-cost GPS/INS system which uses a Kalman filter as sensor data fusion algorithm. A miniaturized INS is coupled with a stand-alone single-antenna single-frequency (L1) GPS-receiver. Since no differential correction (DGPS) or integer ambiguity knowledge is used, the worst case for a tightly-coupled GPS-aided INS is considered. Obviously, applying correctional data would even increase the achieved accuracy of the integrated navigation system. Regarding intertial sensors, only smallest and cheapest ones are used although they where actually not developed for navigation purposes.

2. MEMS-IMU

The considered micro-electromechanical system (MEMS)-based IMU is shown in FIG. 1. It was devel-

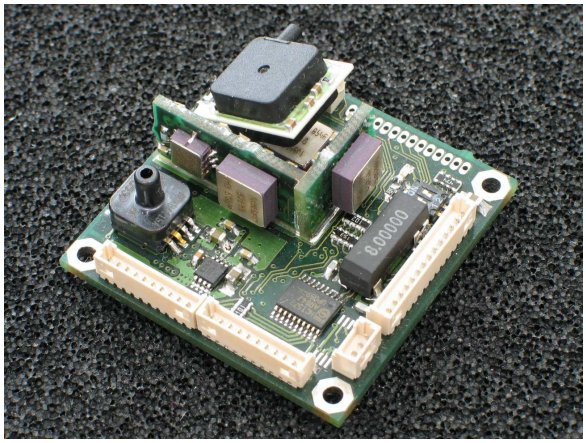

FIG. 1: MEMS-IMU.

oped, built and calibrated at the institute. The design includes three angular rate sensors with a range of ± 300 °/s and two accelerometers with two axes each, providing redundancy for the aircraft's longitudinal axis. The range is 2 g for the horizontal and 10 g for the vertical axis. The nominal data rate for all sensors is 100 Hz. The MEMS-based IMU has a weight of less than 15 grams and a size of $40 \times 40 \times 16$ mm^3. For more details on additional features, technical data and design see [3].

The MEMS-IMU was calibrated using the model introduced in [4]. Goal was the determination of scale factor, bias and misalignment. The temperature influence on the calibration data was not explicitely taken into account. But due to the integration with GPS changes in sensor biases could be estimated by the navigation filter and extracted from the measurements. Drive tests and flight have shown biases of about $0,1 - 0,15$ m/s^2 and $0,6 - 2,3$ °/s. Measurement noise and resolution are sumarized in TABLE 1.

	Noise	Resolution
Accelerometer (2g)	$0.13\ \frac{\mathrm{m}}{\mathrm{s}}/\sqrt{h}$	$0.012\ \frac{\mathrm{m}}{\mathrm{s}^2}$
Accelerometer (10g)	$0.37\ \frac{\mathrm{m}}{\mathrm{s}}/\sqrt{h}$	$0.035\ \frac{\mathrm{m}}{\mathrm{s}^2}$
Gyro	$1.82\ °/\sqrt{h}$	$0.24\ °/s$

TABLE 1: Properties of the MEMS-IMU.

3. GPS/INS-INTEGRATION

3.1 Navigation System Architectures

The easiest method of GPS/INS sensor data fusion is the *loosely-coupled* integration. Here, the INS navigation solutions (from strapdown-algorithm) for position $\mathbf{r}$, velocity $\mathbf{v}$ and attitude $\boldsymbol{\phi}$ are aided by GPS position and velocity measurements (see FIG. 2). Inside the GPS-receiver, raw data (pseudoranges $\boldsymbol{\rho}$, deltaranges $\dot{\boldsymbol{\rho}}$) and satellite ephemeris data are processed to compute these values. This system architecture is easiest to realize because of only very little integration efforts within the sensor data fusion algorithm (navigation filter). GPS and INS can be used independently from each other as stand-alone systems as well. But it has two significant disadvantages. First, signals from at least four satellites must be tracked in order to compute a position and velocity information. Therefore, in phases with less than four satellites no aiding information can be provided by the GPS. This causes increasing navigation errors according to the performance of the INS used. Second, position and velocity determination inside the receiver is often done by a Kalman filter. This results in a time-correlation of these data which can cause problems regarding accuracy and stability of the sensor data fusion filter. But such a serial structure of filters could be considered using a Federated Filter ([see 5; 6; 7]). In addition, the covariance matrices for the GPS-position and velocity vector outputs have no diagonal shape. Therefore, an efficient sequential measurement processing within the sensor data fusion filter is not possible without previous decorrelation.

A second method of GPS/INS sensor data fusion is the *tightly-coupled* integration. For most authors it is characterized by using GPS raw data to aid the INS (see FIG. 3). Some authors name it tightly-coupled only if the INS aids the GPS as well e.g. during satellite acquisition or tracking [8; 9]. Otherwise they call it a *closely-coupled* system [10]. The significant advantage compared to a loosely-coupled system is that even with less than four satellites the INS can be aided by GPS and, hence, the navigation errors in such phases can be decreased. A disadvantage is the increased integration effort. If the GPS-receiver does not output satellite position and velocity they must be computed within the sensor fusion algorithm.

A third method of GPS/INS sensor data fusion is the *ultra-tightly coupled* or *deeply-coupled* integration. Here, the navigation filter directly processes the I & Q samples from the receiver-intern signal processing and closes the signal tracking loops of the receiver. The advantage of this navigation system architecture lays in a higher navigation precision and a lower minimum required GPS signal-to-noise ratio which makes the integrated system more robust against jamming. Hence, this method is of primary importance for military users. The major disadvantage is a higher integration effort compared to a tightly-coupled system. Furthermore, access to the receiver-intern signal processing is necessary which is often limited to the manufacturer. Therfore, this navigation system architecture is not adequate for general users. For more details see [11; 12; 13].

In conclusion, loosely-coupled low-cost GPS/MEMS-INS integration is not very suitable for small UAVs. The main reason is the missing aiding informati-

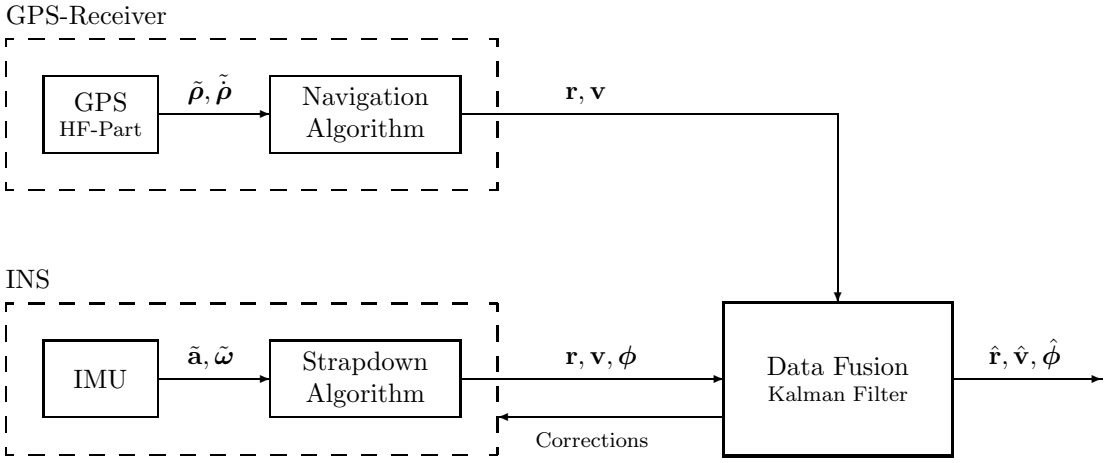

FIG. 2: Loosely coupled GPS/INS-system architecture.

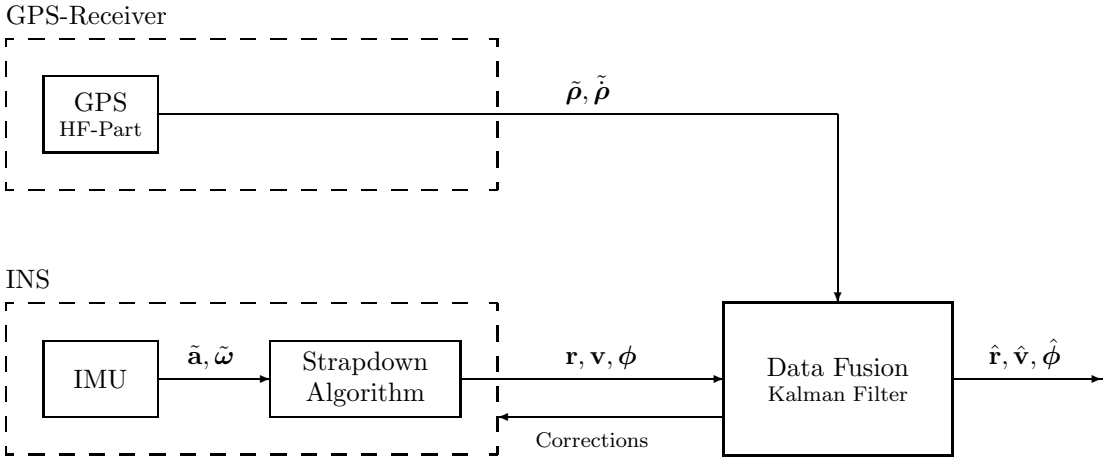

FIG. 3: Tightly coupled GPS/INS-system architecture (here: closely coupled).

on from GPS during high-dynamic flight maneuvers, when there are frequently less than four satellites tracked by the receiver. In addition, a Federated Filter in order to consider the serial structure of receiver-intern and data fusion Kalman filter requires too much computing power. Furthermore, a tightly-coupled system can provide aiding information with less than four tracked satellites and, thus, a more robust navigation solution. On the other hand, more integration effort is necessary. An ultra-tightly or deeply-coupled system is not suitable for the applications considered since no access to the receiver-intern signal processing is given. In conclusion, a tightly-coupled system architecture is the most promising of the methods presented. From now on the paper focuses on tightly-coupled low-cost GPS/MEMS-INS integration for small unmanned aircraft.

3.2 Navigation Filter

As a compromize between achievable accuracy and required computing time a linear error state Kalman filter with the following state vector was used:

$$\mathbf{x} = \begin{bmatrix} \delta\mathbf{r}_g^{eb} & \dots & \text{3 position errors} \\ \delta\mathbf{v}_g^{eb} & \dots & \text{3 velocity errors} \\ \delta\boldsymbol{\phi}^{gb} & \dots & \text{3 attitude angle errors} \\ \delta\boldsymbol{\omega}_b & \dots & \text{3 errors in gyro bias} \\ \delta\mathbf{a}_b & \dots & \text{3 errors in accelerometer bias} \\ \delta(c\,\Delta t) & \dots & \text{1 error in GPS-RX clock error} \\ \delta(c\,\dot{\Delta} t) & \dots & \text{1 error in GPS-RX clock drift} \end{bmatrix}.$$

The indizes $_g$ and $_b$ show that the vector is described in geodetic- and body-frame, respectively. The superscripts ^{eb} and ^{gb} mean body- with respect to (w.r.t.) earth-centered earth-fixed (index $_e$) (ECEF)-frame and b- w.r.t. g-frame, respectively. The δ indica-

tes an error state. The following system matrix of the filter can be derived:

$$\mathbf{F} = \begin{bmatrix} \mathbf{0} & \mathbf{I} & \mathbf{0} & \mathbf{0} & \mathbf{0} & \mathbf{0} \\ \mathbf{F}_{\dot{\mathbf{v}}\mathbf{r}} & \mathbf{F}_{\dot{\mathbf{v}}\mathbf{v}} & -(\hat{\mathbf{T}}_{gb}\tilde{\mathbf{a}}_b)^{\times} & \mathbf{0} & \hat{\mathbf{T}}_{gb} & \mathbf{0} \\ \mathbf{F}_{\dot{\boldsymbol{\phi}}\mathbf{r}} & \mathbf{F}_{\dot{\boldsymbol{\phi}}\mathbf{v}} & \mathbf{F}_{\dot{\boldsymbol{\phi}}\boldsymbol{\phi}} & \hat{\mathbf{T}}_{gb} & \mathbf{0} & \mathbf{0} \\ \mathbf{0} & \mathbf{0} & \mathbf{0} & \mathbf{0} & \mathbf{0} & \mathbf{0} \\ \mathbf{0} & \mathbf{0} & \mathbf{0} & \mathbf{0} & \mathbf{0} & \mathbf{0} \\ \mathbf{0} & \mathbf{0} & \mathbf{0} & \mathbf{0} & \mathbf{0} & \mathbf{F}_{\dot{\mathbf{t}}\mathbf{t}} \end{bmatrix}.$$

Where $\mathbf{T}_{gb}$ is the vector transformation matrix (attitude matrix) from the b- to the g-frame and $\tilde{\mathbf{a}}$ the IMU's accelerometers measurement. The $^{\times}$ denotes cross-product matrix, the $\tilde{}$ measurement and the $\hat{}$ filter estimate or derived from a filter estimate. In case of $\hat{\mathbf{T}}_{gb}$, the attitude matrix is output of the strapdown algorithm but afterwards corrected by filter estimates:

$$\begin{aligned} \mathbf{T}_{gb} &= (\mathbf{I} - \delta\mathbf{T})\,\hat{\mathbf{T}}_{gb} \quad \text{where} \\ \delta\mathbf{T} &= \begin{bmatrix} 0 & -\delta\Psi & \delta\Theta \\ \delta\Psi & 0 & -\delta\Phi \\ -\delta\Theta & \delta\Phi & 0 \end{bmatrix} \\ &= (\delta\boldsymbol{\phi}^{gb})^{\times}. \end{aligned}$$

with $\delta\Phi$, $\delta\Theta$ and $\delta\Psi$ as roll, pitch and yaw angle error, respectively. The submatrices $\mathbf{F_{ij}}$ denote Jacobi-Matrices, e.g.:

$$\mathbf{F}_{\dot{\mathbf{v}}\mathbf{r}} = \frac{\partial\dot{\mathbf{v}}}{\partial\mathbf{r}^{eb}}\ .$$

When dealing with MEMS-sensors some system matrix elements can be neglected compared to others. Hence, the system matrix becomes:

$$(1)\quad \mathbf{F} = \begin{bmatrix} \mathbf{0} & \mathbf{I} & \mathbf{0} & \mathbf{0} & \mathbf{0} & \mathbf{0} \\ \mathbf{0} & \mathbf{0} & -(\hat{\mathbf{T}}_{gb}\tilde{\mathbf{a}}_b)^{\times} & \mathbf{0} & \hat{\mathbf{T}}_{gb} & \mathbf{0} \\ \mathbf{0} & \mathbf{0} & \mathbf{0} & \hat{\mathbf{T}}_{gb} & \mathbf{0} & \mathbf{0} \\ \mathbf{0} & \mathbf{0} & \mathbf{0} & \mathbf{0} & \mathbf{0} & \mathbf{0} \\ \mathbf{0} & \mathbf{0} & \mathbf{0} & \mathbf{0} & \mathbf{0} & \mathbf{0} \\ \mathbf{0} & \mathbf{0} & \mathbf{0} & \mathbf{0} & \mathbf{0} & \mathbf{F}_{\dot{\mathbf{t}}\mathbf{t}} \end{bmatrix}.$$

A tightly-coupled GPS/INS-filter usually processes pseudoranges and delta-ranges (doppler velocities). Here, the delta-ranges will be replaced by time-differenced carrier phases.

Based on the method introduced in [14] and [15], in [16] the algorithm was adapted in order to process time-differenced carrier phase measurements of a stand-alone GPS receiver. It was shown that a filter with time-differenced carrier phases achieves a better velocity and attitude accuracy than a filter using delta-ranges. The method allows to use precise carrier phase measurements without solving the integer ambiguities. Compared to a delayed state Kalman filter (see [17]), commonly used in such a case, this method does not induce additional cross-correlation between measurements at one epoch. Hence, the measurement noise covariance matrix of the filter keeps its diagonal shape. This allows a sequential measurement processing without previous decorrelation and, hence, the avoidance of the matrix inversion in the Kalman gain computation. The following derivation of the Kalman filter measurment matrix is different from the derivation in [16], but agrees with the common approach for error state Kalman filters by arranging estimated less measured value as filter measurement.

The carrier phase measurement provided by the GPS-receiver is $(\tilde{\varphi}+N)\lambda$, where $\tilde{\varphi}$ is the actual phase measurement in [cycles] which is ambiguous because of the unknown integer N, called integer ambiguity. λ is the carrier wavelength (L1: $\approx$ 19 cm). The measurement equation for a carrier phase measurement at epoch t_k (index $_k$) is:

$$(\tilde{\varphi}_k + N)\lambda = \rho_k + c\,\Delta t_k + \varepsilon_k$$

where ρ is the geometrical distance between user antenna and GPS satellite (the range), $c\,\Delta t$ the receiver clock error in [m] and ε the measurement noise containing the common mode errors, multipath error and receiver noise. The time-differenced carrier phase measurement between epoch t_k and t_{k-1} results in:

$$(2)\quad (\tilde{\varphi}_k - \tilde{\varphi}_{k-1})\lambda = \rho_k - \rho_{k-1} + c\,\Delta t_k - c\,\Delta t_{k-1} - \epsilon_k.$$

The noise term ϵ contains the remaining noise after time-differencing. The influence of the common mode errors, which in general is the dominant noise part in ε, on the time-differenced carrier phase reduces significantly if $t_k - t_{k-1}$ is small compared to its correlation time. For example: modelling ε as a 1^{st} order Gauss-Markow signal of standard deviation 5 m and correlation time 1 h (approx. ionosphere error) leads to an ϵ of 0.118 m standard deviation when $t_k - t_{k-1} = 1$ s (1 Hz GPS) [18].

The difference between estimated and measured time-differenced carrier phase shall be provided to the Kalman filter:

$$z_k = (\hat{\tilde{\varphi}}_k - \hat{\tilde{\varphi}}_{k-1})\lambda - (\tilde{\varphi}_k - \tilde{\varphi}_{k-1})\lambda.$$

In order to derive the measurent equation of the filter, with the position changes of satellite $\jmath$ and user antenna $\imath$ w.r.t. the e-frame,

$$\begin{aligned} \Delta\hat{\mathbf{r}}^{e\jmath}_{g,k} &= \hat{\mathbf{r}}^{e\jmath}_{g,k} - \hat{\mathbf{r}}^{e\jmath}_{g,k-1} \\ \Delta\hat{\mathbf{r}}^{e\imath}_{g,k} &= \hat{\mathbf{r}}^{e\imath}_{g,k} - \hat{\mathbf{r}}^{e\imath}_{g,k-1}, \end{aligned}$$

Eq. (2) can be rewritten in the form:

$$(\hat{\tilde{\varphi}}_k - \hat{\tilde{\varphi}}_{k-1})\lambda = \hat{\mathbf{e}}^T_{g,k}(\Delta\hat{\mathbf{r}}^{e\jmath}_{g,k} - \Delta\hat{\mathbf{r}}^{e\imath}_{g,k}) + c\,\hat{\Delta}t_k - c\,\hat{\Delta}t_{k-1}.$$

where $\mathbf{e}$ is the unit vector from the $\imath$-th user antenna to the $\jmath$-th satellite. Neglecting errors in the computed

satellite position, $\Delta\hat{\mathbf{r}}^{ej}_{g,k} = \Delta\mathbf{r}^{ej}_{g,k}$, the filter measurement equation becomes:

$$z_k = \mathbf{e}^T_{g,k}(\Delta\mathbf{r}^{ei}_{g,k} - \Delta\hat{\mathbf{r}}^{ei}_{g,k}) + \delta(c\,\Delta t_k) - \delta(c\,\Delta t_{k-1}) + \epsilon_k.$$

After rewriting this equation as:

$$\begin{aligned} z_k &= \mathbf{e}^T_{g,k}\left[(\mathbf{r}^{ei}_{g,k} - \mathbf{r}^{ei}_{g,k-1}) - (\hat{\mathbf{r}}^{ei}_{g,k} - \hat{\mathbf{r}}^{ei}_{g,k-1})\right] \\ &\quad +\delta(c\,\Delta t_k) - \delta(c\,\Delta t_{k-1}) + \epsilon_k, \end{aligned}$$

the introduction of the vector $\mathbf{l}$, from the IMU (placed in the origin of the b-frame) to the user antenna, leads to:

$$\begin{aligned} z_k &= \mathbf{e}^T_{g,k}\left[(\mathbf{r}^{eb}_{g,k} - \mathbf{r}^{eb}_{g,k-1}) - (\hat{\mathbf{r}}^{eb}_{g,k} - \hat{\mathbf{r}}^{eb}_{g,k-1})\right] \\ &\quad +\mathbf{e}^T_{g,k}\left[(\mathbf{l}_{g,k} - \mathbf{l}_{g,k-1}) - (\hat{\mathbf{l}}_{g,k} - \hat{\mathbf{l}}_{g,k-1})\right] \\ &\quad +\delta(c\,\Delta t_k) - \delta(c\,\Delta t_{k-1}) + \epsilon_k. \end{aligned}$$

The time-differences of the body-frame positions and the receiver clock error can be rewritten in form of time-integrals from t_{k-1} to t_k of the corresponding velocity and receiver clock drift, respectively. Hence, with $\mathbf{e}^T_{g,k} = \hat{\mathbf{e}}^T_{g,k}$ follows:

$$\begin{aligned} z_k &= -\int_{t_{k-1}}^{t_k}\left[\hat{\mathbf{e}}^T_{g,k}\delta\mathbf{v}^{eb}_g - \delta(c\,\dot{\Delta t})\right]dt \\ &\quad +\hat{\mathbf{e}}^T_{g,k}\left[(\mathbf{l}_{g,k} - \mathbf{l}_{g,k-1}) - (\hat{\mathbf{l}}_{g,k} - \hat{\mathbf{l}}_{g,k-1})\right] + \epsilon_k \end{aligned}$$

In order to write the second summand in form of Kalman filter state variables the following steps can be done:

$$\begin{aligned} &(\mathbf{l}_{g,k} - \mathbf{l}_{g,k-1}) - (\hat{\mathbf{l}}_{g,k} - \hat{\mathbf{l}}_{g,k-1}) = \\ &= (\mathbf{T}_{gb,k}\,\mathbf{l}_b - \mathbf{T}_{gb,k-1}\,\mathbf{l}_b) - (\hat{\mathbf{T}}_{gb,k}\,\mathbf{l}_b - \hat{\mathbf{T}}_{gb,k-1}\,\mathbf{l}_b) \\ &= -\delta\mathbf{T}_k\,(\hat{\mathbf{l}}_{g,k} - \hat{\mathbf{l}}_{g,k-1}) - (\delta\mathbf{T}_k - \delta\mathbf{T}_{k-1})\,\hat{\mathbf{l}}_{g,k-1} \\ &= \Delta\hat{\mathbf{l}}_{g,k} \times \delta\boldsymbol{\phi}^{gb} + \Delta T\;\hat{\mathbf{l}}_{g,k-1} \times \delta\dot{\boldsymbol{\phi}}^{gb} \end{aligned}$$

where $\Delta T = (t_k - t_{k-1})$ and $\Delta\hat{\mathbf{l}}_{g,k} = (\hat{\mathbf{l}}_{g,k} - \hat{\mathbf{l}}_{g,k-1})$. With:

$$\delta\dot{\boldsymbol{\phi}}^{gb} \approx \hat{\mathbf{T}}_{gb,k}\,\delta\boldsymbol{\omega}_b$$

can be written:

$$\begin{aligned} &(\mathbf{l}_{g,k} - \mathbf{l}_{g,k-1}) - (\hat{\mathbf{l}}_{g,k} - \hat{\mathbf{l}}_{g,k-1}) = \\ &= \Delta\hat{\mathbf{l}}^{\times}_{g,k}\,\delta\boldsymbol{\phi}^{gb} + \Delta T\;\hat{\mathbf{l}}^{\times}_{g,k-1}\,\hat{\mathbf{T}}_{gb,k}\,\delta\boldsymbol{\omega}_b \end{aligned}$$

and finally:

$$\begin{aligned} z_k &= -\int_{t_{k-1}}^{t_k}\left[\hat{\mathbf{e}}^T_{g,k}\delta\mathbf{v}^{eb}_g - \delta(c\,\dot{\Delta t})\right]dt \\ &\quad +\hat{\mathbf{e}}^T_{g,k}\left(\Delta\hat{\mathbf{l}}^{\times}_{g,k}\,\delta\boldsymbol{\phi}^{gb} + \Delta T\;\hat{\mathbf{l}}^{\times}_{g,k-1}\,\hat{\mathbf{T}}_{gb,k}\,\delta\boldsymbol{\omega}_b\right) \\ &\quad +\epsilon_k \\ &= -\int_{t_{k-1}}^{t_k}\left[\hat{\mathbf{e}}^T_{g,k}\delta\mathbf{v}^{eb}_g - \delta(c\,\dot{\Delta t})\right]dt + \mathbf{H}^{\ddagger}_k\,\mathbf{x}_k + \epsilon_k \end{aligned}$$

where:

$$\begin{aligned} \mathbf{H}^{\ddagger}_k &= \Big[\mathbf{0}^T \quad \mathbf{0}^T \quad \hat{\mathbf{e}}^T_{g,k}\Delta\hat{\mathbf{l}}^{\times}_{g,k} \\ &\qquad \hat{\mathbf{e}}^T_{g,k}\Delta T\;\hat{\mathbf{l}}^{\times}_{g,k-1}\,\hat{\mathbf{T}}_{gb,k} \quad \mathbf{0}^T \quad 0 \quad 0\Big]. \end{aligned}$$

In general, for the integral term one can write:

$$-\int_{t_{k-1}}^{t_k}\left[\hat{\mathbf{e}}^T_{g,k}\delta\mathbf{v}^{eb}_g - \delta(c\,\dot{\Delta t})\right]dt = \int_{t_{k-1}}^{t_k}\mathbf{H}^{\dagger}_k\,\mathbf{x}(t)\,dt$$

where:

$$\mathbf{H}^{\dagger}_k = \left[\begin{array}{ccccccc} \mathbf{0}^T & -\mathbf{e}^T_{g,k} & \mathbf{0}^T & \mathbf{0}^T & \mathbf{0}^T & 0 & 1 \end{array}\right]$$

which can be treated as a constant from t_{k-1} until t_k. With:

$$\mathbf{x}(t) = \boldsymbol{\Phi}_{t,t_{k-1}}\,\boldsymbol{\Phi}_{t_{k-1},t_k}\,\mathbf{x}_k.$$

and the fact that the transition matrix $\boldsymbol{\Phi}_{t_{k-1},t_k}$ is time-invariant it follows that:

$$\begin{aligned} &-\int_{t_{k-1}}^{t_k}\left[\hat{\mathbf{e}}^T_{g,k}\delta\mathbf{v}^{eb}_g - \delta(c\,\dot{\Delta t})\right]dt = \\ &= \mathbf{H}^{\dagger}_k\left(\int_{t_{k-1}}^{t_k}\boldsymbol{\Phi}_{t,t_{k-1}}\,dt\right)\boldsymbol{\Phi}_{t_{k-1},t_k}\,\mathbf{x}_k. \end{aligned}$$

Hence, the Kalman filter measurement equation can be written in the form:

$$z_k = \mathbf{H}_k\,\mathbf{x}_k + \epsilon_k$$

with the measurement matrix:

$$\mathbf{H}_k = \left[\mathbf{H}^{\dagger}_k\left(\int_{t_{k-1}}^{t_k}\boldsymbol{\Phi}_{t,t_{k-1}}\,dt\right)\boldsymbol{\Phi}_{t_{k-1},t_k} + \mathbf{H}^{\ddagger}_k\right].$$

In order to compute $\mathbf{H}_k$, the time integral and the backwards transforming state transition matrix $\boldsymbol{\Phi}_{t_{k-1},t_k}$ are developed stepwise with new IMU-measurements in each step. So the time-integral must be approximated as a sum and computed successively from t_{k-1} to t_k with step time τ, which is equal to the IMU sampling time. n is the number of samples to go from t_{k-1} to t_k, hence: $t_k = t_{k-1} + n\tau$. For $n > 1$:

$$\int_{t_{k-1}}^{t_k}\boldsymbol{\Phi}_{t,t_{k-1}}\,dt \approx \sum_{i=1}^{n}\tau\,\left(\mathbf{I} - \mathbf{F}_{t_{k-1}+(i-1)\,\tau}\,\tau\right). \tag{3}$$

Accordingly, $\boldsymbol{\Phi}_{t_{k-1},t_k}$ can be numerically computed by:

$$\boldsymbol{\Phi}_{t_{k-1},t_k} \approx \prod_{i=1}^{n}\left(\mathbf{I} - \mathbf{F}_{t_{k-1}+i\,\tau}\,\tau\right). \tag{4}$$

In order to account for time delays between GPS and IMU measurements, Eqs. (3) and (4) can be adapted to the problem on hand.

3.3 Observability

The considered system shall be defined in the time-interval T. An initial state $\mathbf{x}_0 = \mathbf{x}(t_0)$ with $t_0 \in T$ is called *observable*, if $\mathbf{x}_0$ can be determined using the measurements $\mathbf{z}$ during a finite time interval $t_0 \leq t \leq t_f$, $t \in T$ [7]. Sometimes complete and non-complete observability are distinguished. In the first case each single state of the state vector can be determined, in the second only a few at maximum. The other states are either only determinable in terms of linear combinations of states or not at all.

Observability is an important factor in GPS/INS-systems although often either not considered or limited to looking at the system matrix $\mathbf{F}$ only. But such results are incomplete. An extensive observability analysis for single and multiple antenna systems was carried out in [19] in terms of similarity transformations. In [20] the results were confirmed by analyzing the observability matrix. In general, the most important result is that only when using at least three antennas with nonlinear position vectors w.r.t. the IMU a complete, motion-free observability is guaranteed. For this, the INS-aiding data of the GPS-receiver output must be accurate enough in order to resolve the antenna positions. Without integer ambiguity solved carrier phase measurements this is not feasible for the small UAVs considered.

Now, an observability analysis of a low-cost single-antenna GPS/INS-system for small UAVs based on the observability matrix will be carried out. It will be focused on position and velocity instead of raw measurements from the GPS since only with four or more satellites an observability can be expected at all. With $\tilde{\boldsymbol{\omega}}$ as angular rate measurement of the IMU and the following nomenclature:

$$\begin{aligned}
\mathbf{a} &= \hat{\mathbf{T}}_{gb}\tilde{\mathbf{a}}_b \\
\mathbf{T} &= \hat{\mathbf{T}}_{gb} \\
\mathbf{l} &= \mathbf{l}_b \\
\mathbf{L} &= \hat{\mathbf{T}}_{gb}\,\mathbf{l}_b \\
\boldsymbol{\Omega}_l &= \hat{\mathbf{T}}_{gb}\,(\tilde{\boldsymbol{\omega}}_b \times \mathbf{l}_b),
\end{aligned}$$

the Kalman filter system matrix becomes:

$$\mathbf{F} = \begin{bmatrix}
\mathbf{0} & \mathbf{I} & \mathbf{0} & \mathbf{0} & \mathbf{0} \\
\mathbf{0} & \mathbf{0} & -\mathbf{a}^{\times} & \mathbf{0} & \mathbf{T} \\
\mathbf{0} & \mathbf{0} & \mathbf{0} & \mathbf{T} & \mathbf{0} \\
\mathbf{0} & \mathbf{0} & \mathbf{0} & \mathbf{0} & \mathbf{0} \\
\mathbf{0} & \mathbf{0} & \mathbf{0} & \mathbf{0} & \mathbf{0}
\end{bmatrix}$$

and the measurement matrixes for position and velocity, $\mathbf{H_r}$ and $\mathbf{H_v}$, respectively:

$$\begin{aligned}
\mathbf{H_r} &= \begin{bmatrix} \mathbf{I} & \mathbf{0} & -\mathbf{L}^{\times} & \mathbf{0} & \mathbf{0} \end{bmatrix} \\
\mathbf{H_v} &= \begin{bmatrix} \mathbf{0} & \mathbf{I} & -\boldsymbol{\Omega}_l^{\times} & -\mathbf{T}\,\mathbf{l}^{\times} & \mathbf{0} \end{bmatrix}.
\end{aligned}$$

Assuming a time-invariant system leads to the following observability matrix:

$$\begin{aligned}
\boldsymbol{\mathcal{O}} &= \left[\frac{\boldsymbol{\mathcal{O}}_{\mathbf{r}}}{\boldsymbol{\mathcal{O}}_{\mathbf{v}}}\right] \\
&= \left[\begin{array}{ccccc}
\mathbf{I} & \mathbf{0} & -\mathbf{L}^{\times} & \mathbf{0} & \mathbf{0} \\
\mathbf{0} & \mathbf{I} & \mathbf{0} & -\mathbf{L}^{\times}\mathbf{T} & \mathbf{0} \\
\mathbf{0} & \mathbf{0} & -\mathbf{a}^{\times} & \mathbf{0} & \mathbf{T} \\
\mathbf{0} & \mathbf{0} & \mathbf{0} & -\mathbf{a}^{\times}\mathbf{T} & \mathbf{0} \\
\hline
\mathbf{0} & \mathbf{I} & \boldsymbol{\Omega}_l & -\mathbf{T}\,\mathbf{l}^{\times} & \mathbf{0} \\
\mathbf{0} & \mathbf{0} & -\mathbf{a}^{\times} & \boldsymbol{\Omega}_l\,\mathbf{T} & \mathbf{T} \\
\mathbf{0} & \mathbf{0} & \mathbf{0} & -\mathbf{a}^{\times}\mathbf{T} & \mathbf{0}
\end{array}\right]
\end{aligned}$$

where $\boldsymbol{\mathcal{O}}_{\mathbf{r}}$ describes the position-only aiding, $\boldsymbol{\mathcal{O}}_{\mathbf{v}}$ the velocity-only aiding and $\boldsymbol{\mathcal{O}}$ the combined position and velocity aiding. When dealing with small UAVs and stand-alone GPS-receivers the leverarm $\mathbf{l}$ can not be resolved by the GPS-measurements. Hence, the leverarm can be neglected which results in the simplified observability matrix:

$$\begin{aligned}
\boldsymbol{\mathcal{O}} &= \left[\frac{\boldsymbol{\mathcal{O}}_{\mathbf{r}}}{\boldsymbol{\mathcal{O}}_{\mathbf{v}}}\right] \\
&= \left[\begin{array}{ccccc}
\mathbf{I} & \mathbf{0} & \mathbf{0} & \mathbf{0} & \mathbf{0} \\
\mathbf{0} & \mathbf{I} & \mathbf{0} & \mathbf{0} & \mathbf{0} \\
\mathbf{0} & \mathbf{0} & -\mathbf{a}^{\times} & \mathbf{0} & \mathbf{T} \\
\mathbf{0} & \mathbf{0} & \mathbf{0} & -\mathbf{a}^{\times}\mathbf{T} & \mathbf{0} \\
\hline
\mathbf{0} & \mathbf{I} & \mathbf{0} & \mathbf{0} & \mathbf{0} \\
\mathbf{0} & \mathbf{0} & -\mathbf{a}^{\times} & \mathbf{0} & \mathbf{T} \\
\mathbf{0} & \mathbf{0} & \mathbf{0} & -\mathbf{a}^{\times}\mathbf{T} & \mathbf{0}
\end{array}\right].
\end{aligned} \tag{5}$$

For the observability analysis three different aiding-cases shall be distingished:

1. Position-only Aiding

Deciding is the matrix $\boldsymbol{\mathcal{O}}_{\mathbf{r}}$. Eq. (5) shows that at maximum it has a rank (Rg) of 12 which can be interpreted as having a linear equation system of only 12 equations but 15 unknowns. The first row of $\boldsymbol{\mathcal{O}}_{\mathbf{r}}$ shows the observability of the position error, the second that of the velocity error. From the fourth row follows that all three gyro bias errors are only observable if $\mathrm{Rg}(\mathbf{a}^{\times}\mathbf{T}) = 3$. Hence, without horizontal acceleration they can not be estimated independently from each other. The third row shows that attitude angle errors and accelerometer bias errors can only be observed as linear combination. Hence, the estimated attitude angle errors contain accelerometer bias errors and vice versa. Without horizontal acceleration the yaw angle error is not observable. Therefore, when dealing with single-antenna GPS/INS-systems for e.g. helicopters an additional aiding sensor, e.g. a magnetometer, is

necessary (see [21]). If the measured horizontal acceleration is significantly smaller than the vertical, which due to Earth gravity is the case for the considered aircraft during cruising flight, the third row gives the following results for the accelerometer biases $\delta a_{b,x}$, $\delta a_{b,y}$ and $\delta a_{b,z}$ and attitude angle errors $\delta\Phi$ und $\delta\Theta$:

- $\delta a_{b,x}$ is not distinguishable from $\delta\Theta$,
- $\delta a_{b,y}$ is not distinguishable from $\delta\Phi$,
- $\delta a_{b,z}$ is better estimable than $\delta a_{b,x}$ and $\delta a_{b,y}$.

Since attitude angle and accelerometer bias errors are not completely observable, for good attitude estimations good-quality accelerometers with preferably small biases are more important than high-quality gyros whose biases are better observable. In the best case the accelerometer biases does not need to be estimated so that the attitude errors become completely observable during horizontal acceleration.

2. Velocity-only Aiding

Deciding is the matrix $\boldsymbol{\mathcal{O}}_{\mathbf{v}}$. Eq. (5) shows that at maximum it has a rank of 9. The zero-column reflects that the position error is not observable. Otherwise, the results of position-only aiding from above are valid.

3. Position and Velocity Aiding

Deciding is the matrix $\boldsymbol{\mathcal{O}}$. Eq. (5) shows that at maximum it has a rank of 12. The velocity-aiding in addition to the position-only aiding has no influence on the observability. Therefore, the results of position-only aiding from above are valid.

4. EXPERIMENTAL VALIDATION

After filter design and testing in simulations, drive tests and flight tests were carried out in order to validate the navigation filter under realistic conditions. In this section the quality of the low-cost GPS/MEMS-INS-system will be related to a FOG-IMU-based GPS/INS-system which presents the navigation reference. It has an attitude accuracy of approximately $0,01°$ (1σ). For the reasons described in section 1, it will be focused on attitude accuracy.

4.1 Drive Tests

Drive tests were carried out with the institute's van. FOG-IMU and MEMS-IMU were mounted on an aluminum plate inside the car, the GPS-antenna on the roof. All necessary data for filter validation were recorded during the drives. The validation was done in post-processing using the navigation filter developed for real-time applications.

The first drive test was 25 min long and went through a rural environment surrounding the research airport of Braunschweig. Groundtrack and number of tracked satellites are shown in FIG. 4. During the first 60 s and the following two phases the van was at rest (with running engine):

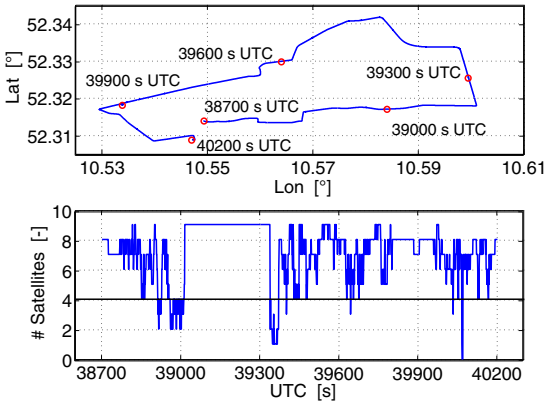

FIG. 4: Groundtrack and number of tracked satellites during drive test (rural environment).

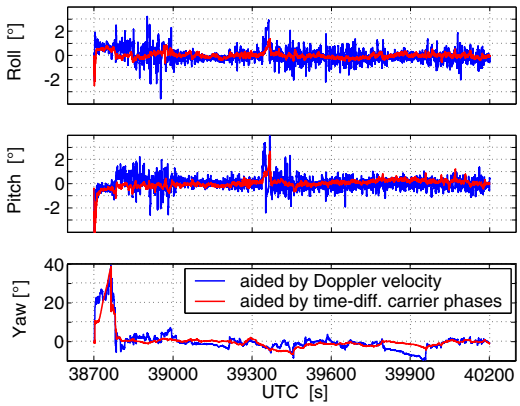

FIG. 5: Attitude angle errors during drive test (rural environment).

1. 100 s from 39100 until 39200 s UTC,
2. 140 s from 39810 until 39950 s UTC.

The attitude error is shown in FIG. 5. It clearly shows the advantage of processing time-differenced carrier phases instead of doppler velocities. The large yaw angle error at the beginning is because it is not observable without horizontal accelerations (see section 3.3). When the drive starts the yaw angle error becomes observable and decreases. An increasing yaw angle error can also be seen during the two phases when the van is at rest. However, it is much smaller than at the beginning. The reason is, that the yaw-gyro bias is also observable during horizontal accelerations only. Therefore, during the first 60 s before the van starts the filter is not able to estimate the bias which causes the large increase of yaw angle error. When the other two standing phases begin, the filter has been able to estimate the yaw-gyro bias. Since it is used to directly correct the gyro measurement, the remaining bias error is much smaller so that the yaw angle error increases much less. Hence, FIG. 5 also shows that processing time-differenced carrier phases leads to a

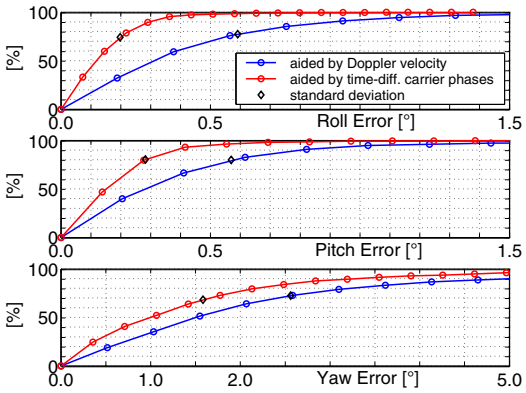

FIG. 6: Cumulative frequency of attitude errors during drive test (rural environment).

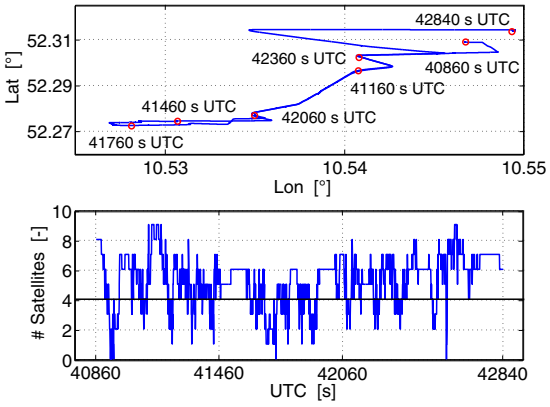

FIG. 7: Groundtrack and number of tracked satellites during drive test (urban environment).

more accurate and robust gyro-bias estimation.

While the time-plot of attitude errors is important for evaluating the filter as provider of flight controller input data, users such as meteorologists are more interested in the frequency of error occurrence. The cumulative frequency of the attitude errors corresponding to FIG. 5 is shown in FIG. 6 neglecting the first 60 s when the vehicle is at rest. Again, processing time-differenced carrier phases leads to better results.

Next, a 33 min urban drive through Braunschweig was done. Groundtrack and number of tracked satellites are shown in FIG. 7. Often less that 4 satellites were tracked because signals were blocked by buildings and other obstacles. The attitude error is shown in FIG. 8. Again, it clearly shows the advantage of processing time-differenced carrier phases instead of doppler velocities by smaller values. Roll and pitch errors are small even during longer phases of less than 4 satellites because they benefit from the Earth acceleration. The yaw angle error becomes larger because of long standing phases.

The attitude accuracies achieved during the drive tests are summarized in TABLE 2. While roll and pitch angle accuracy remain equal or become slightly worse, yaw angle accuracy becomes clearly worse during the urban drive for the reasons described above.

	Rural env.	Urban env.
Roll angle	0.19°	0.27°
Pitch angle	0.28°	0.28°
Yaw angle	1.58°	3.25°

TABLE 2: Attitude accuracy (1σ) during drive tests using time-differenced carrier phases.

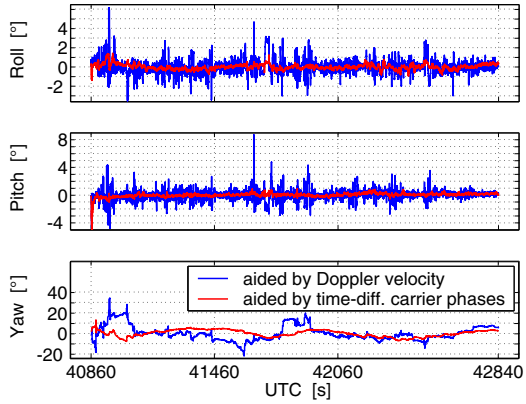

FIG. 8: Attitude angle errors during drive test (urban environment).

4.2 Flight Tests

Flight tests with the institute's GN&C test platform, equipped with the reference and low-cost GPS/INS-system already used in the drive tests, were carried out. The platform is a small unmanned aircraft with 2 m wing span, about 6 kg maximum take-off weight and about 1.5 kg payload capacity. Again, all data were recorded during the flights and afterwards processed with the navigation filter developed for real-time applications.

In order to visualize the flight trajectory, roll angle and number of tracked satellites are shown in FIG. 9. Until 29370 s UTC stationary and accelerated/deccelerated horizontal flights and afterwards, until 29470 s UTC, horizontal flights with alternating roll and pitch were done. After that, the aircraft did horizontal turns with different roll angles until landing.

The attitude error is shown in FIG. 10. The attitude error when using time-differenced carrier phases has a smoother behavior which is important for flight controller input data. But a significant accuracy improve-

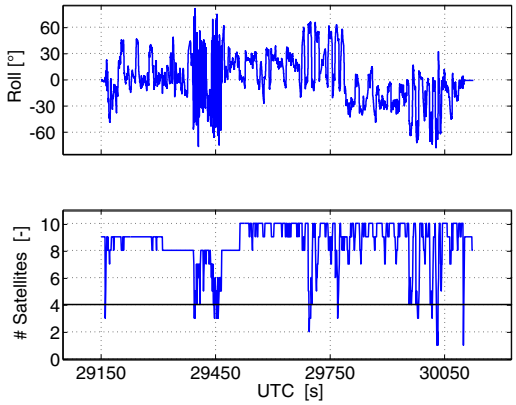

FIG. 9: Roll angle and number of tracked satellites during flight test.

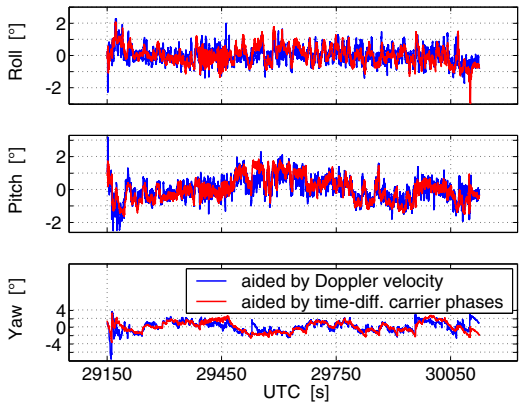

FIG. 10: Attitude angle errors during flight tests.

ment like during the drive tests can not be recognized anymore. This is confirmed by the cumulative frequencies in FIG. 11. As a reason the strong vibrations due to the aircraft engines are assumed, since they cause strong time and cross correlations in the inertial sensor measurements.

The attitude accuracy achieved during the flight test is summarized in TABLE 3. Compared to the drive test results in TABLE 2, there is a small degradation only in roll and pitch angle accuracy (due to vibrations). The yaw angle error becomes smaller due to higher dynamics.

Roll angle	0.54°
Pitch angle	0.71°
Yaw angle	1.22°

TABLE 3: Attitude accuracy (1σ) during flight test using time-differenced carrier phases.

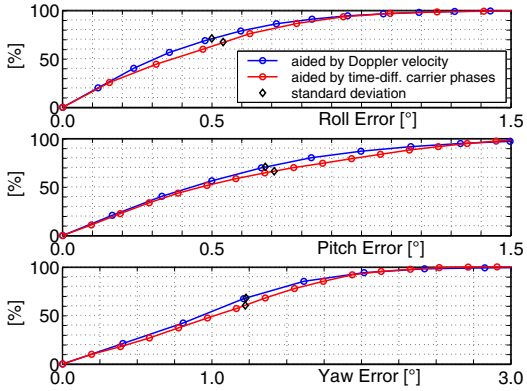

FIG. 11: Cumulative frequency of attitude errors during flight test.

5. SUMMARY

An integrated navigation system was developed and validated in drive tests and flight tests. In this tightly-coupled GPS/INS-system the MEMS-INS was aided by raw data from a commercial low-cost stand-alone single-antenna L1-GPS-receiver. The filter provides reliable and high-frequent state estimates of small unmanned aircraft.

For integration a linear error state Kalman filter of 17 states was developed and simplified for using low-cost sensors. Instead of processing delta-ranges, it was analyzed to replace them by time-differenced carrier phases. The corresponding measurement model for the navigation filter was derived. The observability analysis of the system shows that attitude angle errors and accelerometer biases of the IMU can be estimated only combined in terms of linear combinations.

The experimental validation shows an accuracy (1σ) of 0.89° in tilt and 1.22° in yaw during flight test, 0.34° in tilt and 1.58° in yaw during drive test through rural environment and 0.39° in tilt and 3.25° during drive test through urban environment. In general, drive tests show a significant improvement of attitude accuracy when processing time-differenced carrier phases instead of delta-ranges in the navigation filter. This advantage mostly disappears during the flight tests because of strong vibrations due to the aircraft engines. However, processing time-differenced carrier phases leads to smoother attitude results and, hence, are better qualified for application in flight control systems of small UAVs.

Since no differential correction (DGPS) or integer ambiguity knowledge is used in the GPS, the worst case for a tightly-coupled GPS-aided INS is considered. Obviously, applying correctional data would even increase the achieved accuracy of the integrated navigation system.

6. REFERENCES

1 S. M. Ettinger, M. C. Nechyba, P. G. Ifju, and M. Waszak. Vision-Guided Flight Stablity and Control for Micro Air Vehicles. In *Proceedings of the IEEE International Conference on Intelligent Robots and Systems*, volume 3, pages 2134–40, 2002.

2 H.-W. Schulz, M. Buschmann, T. Kordes, L. Krüger, S. Winkler, and P. Vörsmann. The Autonomous Micro and Mini UAVs of the Carolo-Family. In *Proceedings of the AIAA Infotech@Aerospace (Arlington, VA, September 26-29, 2005)*, American Institute of Aeronautics and Astronautics, 2005.

3 M. Buschmann, A. Heindorf, and P. Vörsmann. MINC: A Miniature Integrated Guidance Navigation and Control System enables in-flight GPS/INS Data Fusion aboard a Micro Aerial Vehicle. In *Proceedings of the 25th ICAS Congress (Hamburg, Germany, September 3-8, 2006)*, 2006.

4 S. Winkler, M. Buschmann, T. Kordes, H.-W. Schulz, and P. Vörsmann. MEMS-based IMU Development, Calibration and Testing for Autonomous MAV Navigation. In *Proceedings of the ION 59th Annual Meeting (Albuquerque, NM, June 23-25, 2003)*, pages 128–134, The Institute of Navigation, 2003.

5 N. A. Carlson. Federated Filter for Distributed Navigation and Tracking Applications. In *Proceedings of the ION 58th Annual Meeting & CIGTF 21st Guidance Test Symposium (Albuquerque, NM, June 24-26, 2002)*, pages 340–353, The Institute of Navigation, 2002.

6 N. A. Carlson. Federated Filter for Fault-Tolerant Integrated Navigation. In J. Niemela, editor, *AGARDograph 331, Aerospace Navigation Systems*, pages 265–280. Neuilly-sur-Seine : AGARD, 1995.

7 G. Minkler and J. Minkler. *Theory and Application of Kalman Filtering*. Magellan Book Company, 1993.

8 B. Vik. *Nonlinear Design and Analysis of Integrated GPS and Inertial Navigation Systems*. PhD thesis, Norwegian University of Science and Technology, Trondheim, Norway, 2000.

9 R. E. Phillips and G. T. Schmidt. *GPS/INS Integration*. NATO AGARD Lecture Series on System Implication and Innovative Applications of Satellite Navigation, LS-207, Paris, France, 1996.

10 C. Kreye, B. Eissfeller, and J. Winkel. Improvements of GNSS Receiver Performance Using Deeply Coupled INS Measurements. In *Proceedings of the ION GPS 2000 (Salt Lake City, UT, September 19-22, 2000)*, pages 844–854, The Institute of Navigation, 2000.

11 P. D. Groves. Performance Analysis and Architectures for INS-Aided GPS Tracking Loops. In *Proceedings of the 2003 ION National Technical Meeting (Anaheim, CA, January 22-24, 2003)*, pages 611–622, The Institute of Navigation, 2003.

12 S. Alban, D. M. Akos, S. M. Rock, and D. Gebre-Egziabher. Performance Analysis and Architectures for INS-Aided GPS Tracking Loops. In *Proceedings of the 2003 ION National Technical Meeting (Anaheim, CA, January 22-24, 2003)*, pages 611–622, The Institute of Navigation, 2003.

13 D. Li and J. Wang. Kalman Filter Design Strategies for Code Tracking Loop in Ultra-Tight GPS/INS/PL integration. In *Proceedings of the 2006 ION National Technical Meeting (Monterey, CA, January 18-20, 2006)*, The Institute of Navigation, 2006.

14 J. L. Farrell. Carrier phase processing without integers. In *Proceedings of the ION 57th Annual Meeting and CIGTF 20th Biennial Guidance Test Symposium(Albuquerque, NM, June 11-13, 2001)*, pages 423–428, The Institute of Navigation, 2001.

15 F. van Graas and J. L. Farrell. GPS/INS - A Very Different Way. In *Proceedings of the ION 57th Annual Meeting and CIGTF 20th Biennial Guidance Test Symposium(Albuquerque, NM, June 11-13, 2001)*, pages 715–721, The Institute of Navigation, 2001.

16 J. Wendel, T. Obert, and G. F. Trommer. Enhancement of a Tightly Coupled GPS/INS System for High Precision Attitude Determination of Land Vehicles. In *Proceedings of the ION 59th Annual Meeting & CIGTF 22nd Guidance Test Symposium (Albuquerque, NM, June 23-25, 2003)*, pages 200–208, The Institute of Navigation, 2003.

17 R. G. Brown and P. Y. C. Hwang. *Introduction to Random Signals and Applied Kalman Filtering*. New York : John Wiley & Sons, 3rd ed. edition, 1997.

18 S. Winkler, H.-W. Schulz, M. Buschmann, and P. Vörsmann. Testing GPS/INS Integration for Autonomous Mini and Micro Aerial Vehicles. In *Proceedings of the ION GNSS 2005 (Long Beach, CA, September 13-16, 2005)*, The Institute of Navigation, 2005.

19 S. Hong and M.-H. Lee. Observability Analysis of GPS Aided INS. In *Proceedings of the ION GPS 2000 (Salt Lake City, UT, September 19-22, 2000)*, pages 2618–2624, The Institute of Navigation, 2000.

20 J. F. Wagner. *Zur Verallgemeinerung integrierter Navigationssysteme auf räumlich verteilte Sensoren und flexible Fahrzeugstrukturen*. Fortschritt-Berichte VDI Reihe 8 Nr. 1008, Düsseldorf: VDI Verlag, 2003.

21 J. Wendel, O. Meister, C. Schlaile, and G. F. Trommer. An Integrated GPS/MEMS-IMU Navigation System for an Autonomous Helicopter. In *Jahrbuch der Deutschen Gesellschaft für Luft- und Raumfahrt 2005, Deutscher Luft- und Raumfahrtkongress 2005 (Friedrichshafen, Germany, September 26-29, 2005)*. Bonn : Deutsche Gesellschaft für Luft und Raumfahrt, 2005.